Neurotherapeutics (2021) 18:2021–2039
https://doi.org/10.1007/s13311-021-01072-z

ORIGINAL ARTICLE

Loss of CC2D1A in Glutamatergic Neurons Results in Autistic-Like Features in Mice

Cheng-Yi Yang[1] · Yu-Chieh Hung[1] · Kuan-Hsiang Cheng[1] · Pin Ling[2] · Kuei-Sen Hsu[1,3]

Accepted: 5 June 2021 / Published online: 16 June 2021

Abstract

Biallelic loss-of-function mutations in Coiled-coil and C2 domain containing 1A (CC2D1A) cause autosomal recessive intellectual disability, sometimes comorbid with other neurodevelopmental disabilities, such as autism spectrum disorder (ASD) and seizures. We recently reported that conditional deletion of *Cc2d1a* in glutamatergic neurons of the postnatal mouse forebrain leads to impaired hippocampal synaptic plasticity and cognitive function. However, the pathogenic origin of the autistic features of CC2D1A deficiency remains elusive. Here, we confirmed that CC2D1A is highly expressed in the cortical zones during embryonic development. Taking advantage of Cre-LoxP-mediated gene deletion strategy, we generated a novel line of *Cc2d1a* conditional knockout (cKO) mice by crossing floxed *Cc2d1a* mice with *Emx1*-Cre mice, in which CC2D1A is ablated specifically in glutamatergic neurons throughout all embryonic and adult stages. We found that CC2D1A deletion leads to a trend toward decreased number of cortical progenitor cells at embryonic day 12.5 and alters the cortical thickness on postnatal day 10. In addition, male *Cc2d1a* cKO mice display autistic-like phenotypes including self-injurious repetitive grooming and aberrant social interactions. Loss of CC2D1A also results in decreased complexity of apical dendritic arbors of medial prefrontal cortex (mPFC) layer V pyramidal neurons and increased synaptic excitation/inhibition (E/I) ratio in the mPFC. Notably, chronic treatment with minocycline rescues behavioral and morphological abnormalities, as well as E/I changes, in male *Cc2d1a* cKO mice. Together, these findings indicate that male *Cc2d1a* cKO mice recapitulate autistic-like phenotypes of human disorder and suggest that minocycline has both structural and functional benefits in treating ASD.

Keywords CC2D1A · Autism spectrum disorder · Medial prefrontal cortex · Excitation/inhibition balance · Minocycline

Introduction

Coiled-coil and C2 domain containing 1A (CC2D1A) is an evolutionarily conserved scaffold protein, which routes the signals to multiple intracellular signaling pathways, including nuclear factor-κB [1, 2], 3-phosphoinositide-dependent protein kinase 1/Akt [3], cAMP/cAMP-dependent protein kinase/phosphodiesterase 4D [4–6], and Rac1 [7], to regulate distinct cellular functions. *Cc2d1a* mRNA and protein expression is highly enriched in neurons of the cerebral cortex, hippocampus, basal ganglia, and hypothalamus [7–9]. Loss-of-function mutations in the human *Cc2d1a* gene result in a variable spectrum of neurodevelopmental disorders, including intellectual disability, autism spectrum disorder (ASD), and seizures [8, 10, 11]. These disorders are often comorbid with each other. Given that the homozygous *Cc2d1a* null mice die postnatally within a few hours [4] or days [12] after birth due to respiratory distress, *Cc2d1a* conditional knockout (cKO) mice have been used extensively to verify its function. Previous studies from our and other groups have consistently demonstrated that mice with conditional postnatal removal of CC2D1A in forebrain glutamatergic neurons (*Camk2α*-Cre::*Cc2d1a*$^{f/f}$, *Camk2α-Cc2d1a* cKO) have recapitulated several features of the human disorders and, despite a subtle overall degree of impairment, they show behavioral deficits such as impaired cognitive and social function, hyperactivity, compulsivity, and altered

✉ Kuei-Sen Hsu
richard@mail.ncku.edu.tw

[1] Institute of Basic Medical Sciences, College of Medicine, National Cheng Kung University, Tainan 70101, Taiwan

[2] Department of Microbiology & Immunology, College of Medicine, National Cheng Kung University, Tainan 70101, Taiwan

[3] Department of Pharmacology, College of Medicine, National Cheng Kung University, No. 1, University Rd., Tainan 70101, Taiwan

anxiety-like behaviors [7, 13, 14]. While *Cc2d1a* is classified as a strong ASD-risk gene (category 2) in the Simons Foundation Autism Research Initiative (SFARI), the role of *Cc2d1a* in brain development and the biological significance of ASD-associated *Cc2d1a* mutations in the etiology of ASD remain largely unknown.

Previous studies have demonstrated that *Cc2d1a* mRNA expression in the developing mouse cerebral cortex starts as early as embryonic day (E) 12.5, increases throughout development with a peak at postnatal (P) 3, and remains enriched into adulthood [8, 10, 15]. Most of the work on behavioral abnormalities caused by genetic deletion of *Cc2d1a* is based on *Camk2α-Cc2d1a* cKO mice, which exhibit postnatal knockout of CC2D1A in forebrain excitatory neurons. Considering that *Cc2d1a* mRNA expression is enriched during embryonic cortical development, we wondered whether early embryonic deletion of CC2D1A from cortical pyramidal neurons may obtain more realistic behavioral changes in cKO mice. The goals of this study were twofold. First, we aimed to establish a novel *Cc2d1a* cKO mouse line for studying the link between CC2D1A deficiency and ASD. Second, as there remains a need for effective treatment for ASD, we aimed to use this mouse model to evaluate the effect of pharmacological intervention for treating autistic-like behaviors. Since Emx-1 is expressed in both progenitor cells and postmitotic glutamatergic neurons [16], we used the *Emx-1* gene to drive expression of the Cre recombinases. By using the *Emx-1*-Cre strain, we were able to ablate CC2D1A expression in forebrain glutamatergic neurons from an early time point and therefore observe changes in brain development and behavioral phenotypes. Interestingly, a recent study suggested that chronic minocycline treatment can improve neuronal structure and function associated with behavioral deficits in fragile X mental retardation 1 (*Fmr1*) knockout mice [17]. As individuals with fragile X syndrome constitute 2–6% of all individuals with ASD [18] and *Fmr1* knockout mice display several autistic-like core symptoms [19], minocycline may be potentially effective in treating ASD. These findings motivated us to further investigate whether chronic minocycline treatment can improve synaptic and behavioral abnormalities in *Cc2d1a* cKO mice. Here, we reported the creation of homozygous *Cc2d1a* cKO mice by crossing mice harboring a floxed *Cc2d1a* allele with the *Emx*1-Cre transgenic line and found that these mice were viable and fertile but showed autistic-like behaviors, including self-injurious repetitive grooming and aberrant social interactions. In addition, loss of CC2D1A resulted in an increase in synaptic excitation to inhibition (E/I) ratio in layer V pyramidal neurons of the medial prefrontal cortex (mPFC). Importantly, chronic treatment with minocycline ameliorates autistic-like features in *Cc2d1a* cKO mice. Our results demonstrate the validity of the *Cc2d1a* cKO as a mouse model for ASD and provide a potential therapeutic strategy for the treatment of CC2D1A-dependent ASD.

Material and Methods

Subjects

Experiments were conducted in compliance with the guidelines by National Institutes of Health for the Care and Use of Laboratory Animals, under protocols approved by the Institutional Animal Care and Use Committee at National Cheng Kung University. Mice were housed in groups of four in a temperature- (25 ± 1 °C) and humidity-controlled room on a 12/12-h light–dark cycle with free access to food and water. The *Cc2d1a* floxed mouse ($Cc2d1a^{f/f}$) line with Cre-dependent excision of exon 12–14 was used for the generation of cKO mice [7]. *Emx*1-Cre (no. 005628) mice were obtained from Jackson Laboratories and maintained in the C57BL/6 J background. *Cc2d1a* cKO mice were generated by crossing *Emx*1-Cre transgenic mice with homozygous $Cc2d1a^{f/f}$ mice. $Cc2d1a^{f/f}$ mice were used as the wild-type (WT) littermates for comparison with homozygous *Cc2d1a* cKO mice. Mice were genotyped by a PCR-based method using genomic DNA isolated from tail samples. Primers used are as follows: forward (5′-GCGGTCTGGCAGTAAAAACTATC-3′) and reverse (5′-GTGAAACAGCATTGCTGTCACTT-3′). While sex-specific behavioral deficits were reported in *Cc2d1a*-deficient mice [6], only male mice were used for experiments throughout the study. The exclusion of female mice from studies because of estrous cycle variability may increase variance relative to males.

Behavioral Assays

All animal behavioral studies were conducted blind to genotype. Mice were allowed to habituate to the testing room for at least 1 h prior to testing. Eight- to twelve-week-old male mice were used for experiments. To avoid potential carryover effects, all animals are used only once throughout the study. The apparatus was thoroughly cleaned with 70% ethanol after each trial.

Open-Field Test

The open-field (OF) test was conducted as previously described [20]. Briefly, each mouse was placed in the center of the test chamber consisted of a square ground area

(42 cm × 42 cm) with 42 cm surrounded non-reflective high wall and allowed to freely explore the arena for 10 min under a dimmed illumination (10 lx). The behavior of the animals was videotaped, tracked, and analyzed with the EthoVision XT video tracking systems. The percentage of time spent in the center (25%) of the arena and the total distance traveled in the OF were measured.

Light/Dark Box Test

The light/dark box (LDB) test was carried out as previously described [21]. Each mouse was placed into an apparatus (30 cm × 30 cm) consisted of a large illuminated compartment (two thirds, ~ 250 lx) and a small dark safe compartment (one third, ~ 5 lx) divided by a partition with door for 10 min. The behavior was videotaped and analyzed using the EthoVision XT video tracking systems.

Marble Burying Test

The marble buried test was conducted as previously described [22]. Mice were individually placed into a standard mouse cage (37.5 cm × 17 cm × 18 cm) filled to a depth of 5 cm fresh corncob bedding material. After allowing 30 min for habituation, 15 marbles were placed evenly throughout the cage. Each mouse was allowed to explore undisturbed for 30 min, and, afterward, the number of successfully buried marbles was counted. A marble was considered buried if more than 2/3 of its depth were covered. The marbles were cleaned with 70% ethanol after each trial.

Repetitive Behavior

The repetitive behavior was performed as previously described [23]. Each mouse was initially placed into a novel home cage with clean bedding for 5 min for habituation. After habituation period, the behavior was videotaped for 10 min. The duration of self-grooming and digging was measured manually. Self-grooming was defined as rubbing, scratching, and licking any part of body.

Three-Chamber Sociability Test

The three-chamber sociability test was performed as previously described [20]. The apparatus was a rectangular, three-chambered box fabricated from clear polycarbonate (60 cm × 40 cm × 22 cm). Dividing walls had retractable doorways that allowed access into each chamber. Each mouse was initially placed into the chambers and allowed to freely explore for 10 min for habituation. After habituation phase, a juvenile male mouse (stimulus), which had no previous contact with the subject mice, was placed in a wire cage of left or right chamber (systemically alternated), and an identical wire cage containing a neutral object was placed in the other chamber. The subject mouse was placed into the middle chamber and allowed to freely explore three chambers for 5 min. The behavior of the animals was videotaped and analyzed using the EthoVision XT video tracking systems. The time that the test subject spent investigating each wire cage was measured. For analyzing sociability, the recognition index was calculated as [(time exploring the social stimulus – time exploring the inanimate object)/(time exploring the objects in both social stimulus and inanimate object) × 100%].

Olfaction Test

The olfactory habituation/dishabituation test was performed as previously described [23]. To present odors to the subject mice, cottons were dipped in water, citrate, and the bottom of unfamiliar cage (social). The subject mice were initially habituated in a clean-bedded cage for 10 min. After habituation, a 35-mm culture dish with odor-dipped cotton was placed into the cage. Each odor was presented for 2 min with 1 min intertrial interval for 3 consecutive trials. Close sniffing within 2 cm was counted as the time spent sniffing. The behaviors of the animals were videotaped and measured by the researcher.

Y-maze Test

Spontaneous alteration behavior was measured on a Y-maze apparatus, composed of three identical arms (arms A, B, and C: 30 cm × 5 cm × 15 cm) at an angle of 120° with each other. The subject mice were placed into the Y-maze at the same end of arm A to freely explore for 10 min (5 min of habituation and 5 min of testing). Sequential exploring three different arms (ex: A > B > C) was considered as a spontaneous alteration. The percentage of spontaneous alteration was calculated by the spontaneous alterations in the total exploring sequence. For example, B > C > A > C > A > C > B, total five sequence (BCA, CAC, ACA, CAC, ACB), had two spontaneous alterations (BCA and ACB), and the percentage was calculated as 40%. The behavior was videotaped and measured by researcher manually.

Reciprocal Social Interaction Test

The reciprocal social interaction test was conducted as previously described [23]. Each mouse was initially allowed to freely explore in a clean cage with clean bedding for 10 min.

After the habituation period, an age-matched male mouse (stimulus) was placed into the cage for freely social interaction for 2 min. The direct social interaction, including genital, face, body sniffing, close approaching, and allogrooming to the stimulus mice, was analyzed using the EthoVision XT video tracking systems.

Nesting Test

The nest-building behavior was analyzed according to the protocol described by Deacon [24]. Approximately 1 h before the dark phase of the light/dark cycle, mice were moved to clean cages and housed individually overnight with food and water freely available. One cotton nestlet was added in the same location of each cage. After 20 h, the nests formed were assessed to generate a nest quality score of 0–5: 0, the nestlet is nearly untouched (> 99% intact); 1, the nestlet is slightly torn up (> 90% intact); 2, the nestlet is partially shredded (50–90% intact); 3, the nestlet is mostly torn up (50–10% intact); 4, the nestlet is mostly shredded (< 10% intact) but flat, with nest walls higher than the mouse body height (< 50% of its circumference); 5, a nearly perfect nest, almost entirely torn up (< 10% intact) with nest walls higher than the mouse body height (> 50% of its circumference). For scores 1–3, 0.5 was added if there was an identifiable nest site.

Rotarod Test

The accelerating rotarod test was performed. Briefly, the subject mice were placed onto the rotarod for 6 trials, 3 trials were performed within a day, for 2 days. Each trial accelerates from 4 to 40 rpm in 300 s. Each trial stopped when the subject mice fell off the rod, and the latency to fall was recorded by the Rotarod Model LE8505 (Panlab, Harvard Apparatus).

Home Cage Activity

After habituation to their home cages for at least 2 days, the subject mice were individually acclimated to the testing environment in a clean cage with clean bedding for 1 h. After acclimation, mice were returned to their home cage and videotaped for 10 min. The behavior of the animals was videotaped, tracked, and analyzed with the EthoVision XT video tracking systems.

Immunohistochemistry

For embryonic studies, embryos were removed from deeply anesthetized pregnant mice for cryosection. After removal, embryonic heads were decapitated and immersed in 4% paraformaldehyde (PFA) in 0.1 M PBS, pH 7.4 overnight at 4 °C, and then incubated in 30% sucrose for cryoprotection before slicing. For postnatal studies, deeply anesthetized mice were perfused transcardially with 4% PFA in 0.1 M PBS, pH 7.4, and brains were rapidly removed for fixation and sucrose cryoprotection. Embryonic brains were embedded in OCT (Leica) and frozen in − 80 °C. The coronal sections containing the mPFC were cut at 20 µm using a freezing microtome. The sections were mounted on gelatin-coated slides and allowed to dry over-night at room temperature. The slides were heated in citrate buffer at 95 °C for 30 min, washed with 0.4% Triton X-100 in PBS, and then incubated in blocking buffer containing 3% goat serum in PBS. The slides were incubated in the primary antibodies: anti-CC2D1A (1:200; generated by Dr. P. Ling laboratory), anti-Nestin (1:200; Millipore, MAB353), anti-Doublecortin (1:200; Millipore, AB2253), anti-Ctip2 (1:200; Abcam, ab18465), anti-Brn2 (1:200; GeneTex, GTX114650), anti-Sox2 (1:200; Abcam, ab97959), anti-CamkIIα (1:1000; Thermo Fisher Scientific, MA1-048), or anti-glial fibrillary acidic protein (GFAP; 1:200; Zymed, 13–0300) overnight at 4 °C. Finally, the slides were washed three times with 0.4% Triton X-100 in PBS, and then incubated in secondary Alexa Fluor 488 (Molecular Probes) or Alexa Fluor 568 antibodies (Molecular Probes) for 2 h at room temperature. Sections were mounted with ProLong Gold Antifade Reagent (Invitrogen). Images were acquired on an Olympus FluoView FV3000 confocal microscope. All images were analyzed by NIH ImageJ software, and all the parameters used were kept consistent during capturing.

Western Blotting

The microdissected tissue samples were lysed in homogenate buffer (Thermo) containing a cocktail of protein phosphatase and protease inhibitors and ground with a pellet pestle (Kontes glassware). Samples were sonicated and then centrifuged at 15,000 × *g* at 4 °C for 15 min. The quantitative samples were separated by 8% SDS-PAGE gel, and then transferred to a nitrocellulose membrane for blotting. The membranes were washed in TBS with 0.1% Tween 20 (TBST) and blocked in TBST containing 3% BSA for 1 h, and then probed with the antibodies that recognize CC2D1A (1:1000; Proteintech, 16,816–1-AP) or β-actin (1:1000; Millipore, MAB1501) overnight at 4 °C. After washes, the membranes were incubated with HRP-conjugated secondary antibody for 1 h and developed using the Luminata™ Crescendo Western HRP Substrate (Millipore). Immunoblots were analyzed by densitometry using Bio-profil BioLight PC software (Vulber Lourmat).

BrdU Immunostaining

The thymidine analog 5-bromo-2′-deoxyuridine (BrdU, 50 mg/kg; Sigma-Aldrich) was intraperitoneally injected into pregnant female mice. For BrdU incorporation of cell proliferation assay at E12.5, embryonic brains were harvested 2 h after BrdU injection and then immersed in 4% PFA in 0.1 M PBS. For neural migration assay, BrdU was injected at E14.5 and then brains were fixed with 4% PFA in 0.1 M PBS at P7. Brains were rapidly removed for fixation and sucrose cryoprotection. The coronal sections containing the mPFC were cut at 20 µm using a freezing microtome. Sections were immersed in citrate buffer at 95 °C for 30 min, and then incubated in 2 N HCl at 37 °C for 30 min. Afterward, sections were rinsed in 0.1 M Na borate (pH 8.5) at 25 °C for 5 min and incubated with primary antibody against BrdU (1:200; Millipore, MAB4072) overnight at 4 °C. Sections were then washed and incubated with secondary antibody Alexa Fluor 488 for 2 h at room temperature. Images were captured by Olympus FluoView FV3000 confocal microscope. Quantification of BrdU numbers was performed by using Imaris image analysis software. Every sixth section covering anterior forebrain in embryo or the mPFC in P7 mice was calculated.

Slice Preparations and Electrophysiological Recordings

Slice preparations and whole-cell patch-clamp recordings were conducted as previously described [25]. Briefly, 8–12-week-old mice were deeply anesthetized and decapitated. The brains were removed quickly and placed in ice-cold slicing solution containing the following (in mM): 234 sucrose, 2.5 KCl, 0.5 $CaCl_2$, 7 $MgCl_2$, 25 $NaHCO_3$, 1.25 NaH_2PO_4, and 11 glucose at pH 7.3–7.4 and equilibrated with 95% O_2–5% CO_2. Slices containing mPFC (250 µm) were sliced using a vibratome (Leica Microsystems, VT1200S) and transferred to a holding chamber with artificial cerebrospinal fluid (aCSF) containing the following (in mM): 117 NaCl, 4.7 KCl, 2.5 $CaCl_2$, 1.2 $MgCl_2$, 25 $NaHCO_3$, 1.2 NaH_2PO_4, and 11 glucose at pH 7.3–7.4 and equilibrated with 95% O_2–5% CO_2, and then rest at room temperature (~25 °C) for 1 h at least.

For electrophysiological recordings, one slice was transferred to a submersion-type recording chamber and continuously perfused with oxygenated aCSF at a flow rate of 2–3 ml/min at ~ 32 °C on a fixed stage. Whole-cell patch-clamp recordings were made from visualized layer V pyramidal neurons of the prelimbic mPFC subregion using an Axopatch 200B amplifier (Molecular Devices). Data acquisition and analysis were performed using a digitizer (Digidata 1440A) and pCLAMP 9 software (Molecular Devices). For presynaptic stimulation, a bipolar stainless steel stimulating electrode was placed on layer II/III of the mPFC. For measuring excitatory postsynaptic current (EPSC) and inhibitory postsynaptic current (IPSC) input–output curve, Eθ was defined as the minimal intensity to evoke an EPSC, and 5 repetitions were collected at each stimulus intensity. All stimulation was conducted at 0.033 Hz to avoid inducing synaptic plasticity. Excitatory postsynaptic current/inhibitory postsynaptic current (EPSC/IPSC) ratio was calculated as the peak EPSC at − 65 mV divided by the IPSC amplitude at 0 mV. The composition of intracellular solution was (in mM): 110 Cs-gluconate, 10 $CsCl_2$, 1 EGTA, 1 $CaCl_2$, 10 HEPES, 1 Mg-ATP, 1 QX-314, and 0.5% w/v biocytin (pH 7.2 adjusted with CsOH). For recording miniature EPSCs (mEPSCs) and miniature IPSCs (mIPSCs), mPFC layer V neurons were held in voltage-clamp mode at a holding potential of − 60 and + 10 for excitatory and inhibitory signals respectively, and tetrodotoxin (1 µM) was added to the bath. The composition of internal solution was (in mM): 100 mM Cs-gluconate, 5 mM CsCl, 10 mM HEPES, 2 mM MgCl2, 1 mM CaCl2, 11 mM BAPTA, 4 mM ATP, 0.4 mM GTP (pH 7.2 adjusted with CsOH). Data were analyzed off-line using a commercially available software (Mini Analysis 4.3; Synaptosoft, Leonia, NJ) as previously described [25]. Means were calculated from 3-min epochs recorded. The cumulative probability plots were constructed to compare the effects of the CC2D1A deletion on the distribution of amplitude and inter-event intervals from mEPSCs and mIPSCs. Detection threshold for analysis was set at three times the root mean square of the background noise, and each event was further confirmed by visual inspection after detection. To assess cell stability, series and input resistances were continuously monitored throughout the experiment with a 5 mV depolarizing step given after every afferent stimulus, and data were excluded from analysis if resistance changed by more than 20%.

Structure Reconstruction and Sholl Analysis

Brain slices loaded with biocytin in mPFC layer V pyramidal neurons were collected and rapidly fixed in 4% paraformaldehyde (PFA) in 0.1 M PBS, pH 7.4 overnight at 4 °C. Biocytin-loaded neurons were visualized by incubating with streptavidin-conjugated Alexa 568 overnight. Brain slices were washed with 0.4% Triton X-100 in PBS,

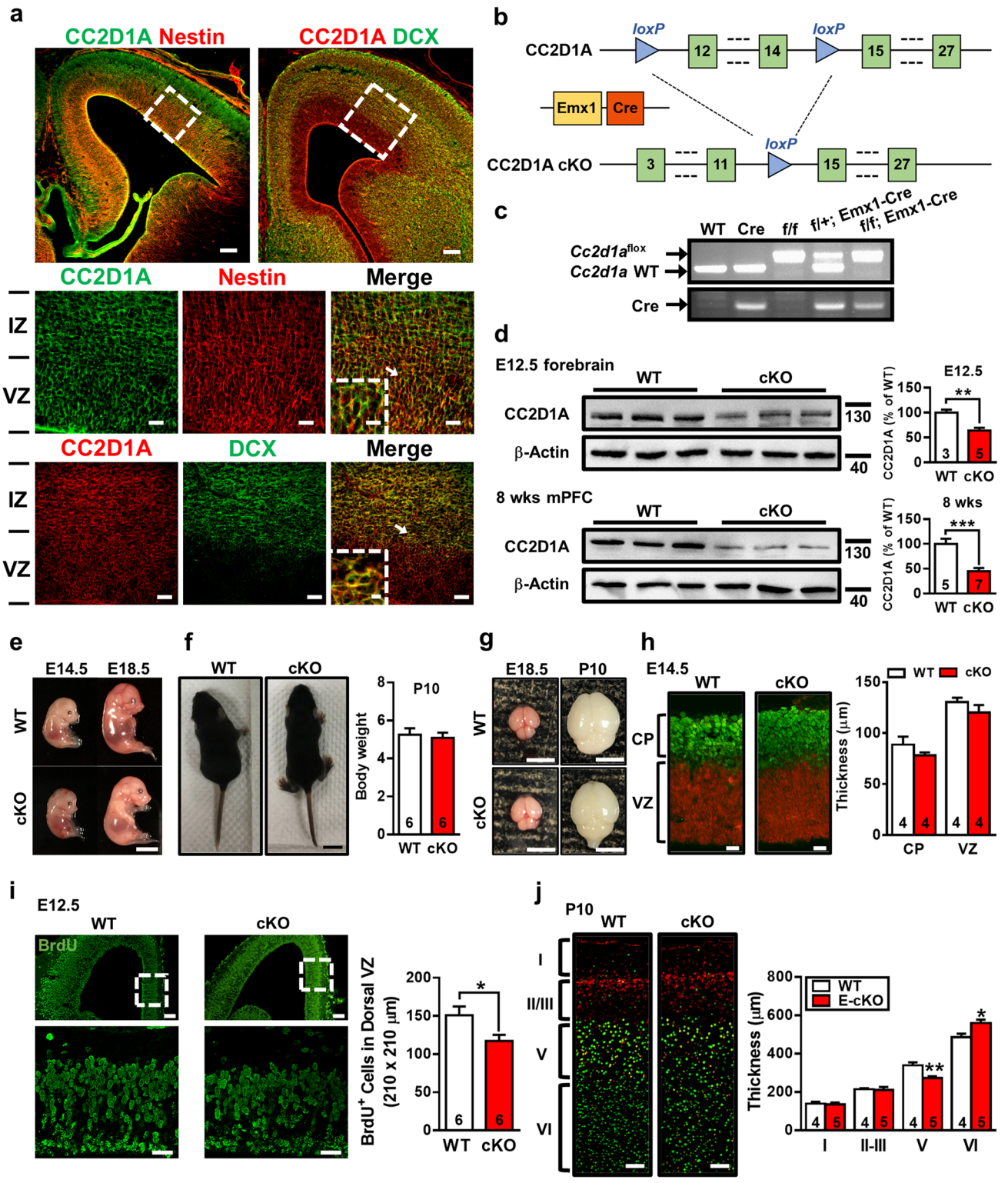

and then mounted onto the slide. Images were captured by Olympus FluoView FV3000 confocal microscope. To evaluate dendritic formation for pyramidal neurons, biocytin-labeled mPFC layer V pyramidal neurons were reconstructed by a computer-assisted neuron-tracing system (Neurolucida, MBF Bioscience Williston, VT), and

◂**Fig. 1** CC2D1A deficiency impairs development of cerebral cortex. **a** Representative double-immunofluorescence images show colocalization of CC2D1A (green) with the neural stem/progenitor cell marker nestin (left) or the immature neuron marker doublecortin (DCX; right) in the mouse brain at embryonic day (E)14.5. Middle and bottom panels are higher-power views of the boxed areas in the upper panels. Higher power views of arrowed areas are shown in the insets. Scale bars: top, 100 µm; middle, 20 µm (boxed area: 10 µm); bottom, 30 µm (boxed area: 5 µm). Images are representative of $n=4$ mice. **b** Schematic representation of recombinant *Cc2d1a* construct; floxed allele enables Emx1-Cre mediated deletion of exon 12–14. **c** PCR screening of tail-derived genomic DNA for selection of wild-type (WT), Emx1-Cre, $Cc2d1a^{f/f}$, heterozygous ($Cc2d1a^{f/+}$; Emx1-Cre) and homozygous ($Cc2d1a^{f/f}$; Emx1-Cre) cKO mice. Images are representative of $n=4$ mice for each genotype. **d** Western blot detection of CC2D1A protein levels in the forebrain at E14.5 ($t_{(6)}=4.14$, $p=0.006$, WT, $n=3$; cKO, $n=5$; two-tailed unpaired Student's t test) and the mPFC at 8 weeks old ($t_{(10)}=4.74$, $p<0.001$, WT, $n=5$; cKO, $n=7$; two-tailed unpaired Student's t test) of the indicated genotypes. **e** Representative photographs showing the body size of WT and cKO mice at E14.5 and E18.5. Scale bar, 5 mm. **f** Representative photographs and summary bar graph depicting the body weight of WT and cKO mice at postnatal day (P)10 ($t_{(10)}=0.38$, $p=0.71$, $n=6$ in each group; two-tailed unpaired Student's t test). Scale bar, 1 cm. **g** Representative photographs showing the entire brain of WT and cKO mice at E18.5 and P10. Scale bar, 5 mm. **h** Representative double immunofluorescence staining for Ctip2 (green) and SOX2 (red) in cerebral cortices from WT and cKO mice at E14.5. Scale bar, 20 µm. Summary bar graph depicting the thickness of the cortical plate (CP; $Ctip2^+$ neurons on the total of $DAPI^+$ cells; $t_{(6)}=1.23$, $p=0.11$, $n=4$ in each group; two-tailed unpaired Student's t test) and ventricular zone (VZ; $SOX2^+$ neurons on the total of $DAPI^+$ cells; $t_{(6)}=1.23$, $p=0.22$, $n=4$ in each group; two-tailed unpaired Student's t test). **i** Representative images of BrdU labeling in cerebral cortices from WT and cKO mice at E12.5. Scale bars: top, 100 µm; bottom, 30 µm. Bottom panels are higher-power views of the boxed areas in the upper panels. Summary bar graph depicting the total number of proliferating ($BrdU^+$) cells in the dorsal VZ of WT and cKO mice at E12.5 ($t_{(10)}=2.379$, $p=0.04$, $n=6$ in each group; two-tailed unpaired Student's t test). **j** Representative double immunofluorescence staining for Ctip2 (layer V and VI marker; green) and Brn2 (layer II-III and V marker; red) in cerebral cortices from WT and cKO mice at P10. Scale bar, 100 µm. A significant change in the thickness of layer V ($t_{(7)}=3.79$, $p=0.006$; two-tailed unpaired Student`s t test) and VI ($t_{(7)}=2.91$, $p=0.02$; two-tailed unpaired Student's t test) was observed in cKO mice ($n=5$) compared with WT mice ($n=4$). Data are represented as mean ± SEM. The total number of animal examined is indicated by n. $^*p<0.05$, $^{**}p<0.01$ compared with WT group

the complexity of dendritic arbor was quantified by Sholl analysis as previously described [7]. A series of concentric rings at 10 mm intervals were centered on the soma, and the number of branches intersecting each ring was counted. For spine density assay, the secondary and the tertiary branches of biocytin-labeled mPFC layer V pyramidal neuron were captured by Olympus FluoView FV3000 confocal microscope equipped with a 100 × 1.25 NA oil-immersion objective. The numbers of spines were counted with 30 µm dendrite segments and presented as the number of spines in 30 µm.

Drug Treatment

Minocycline (30 mg/kg; Sigma-Aldrich) was provided in dam's drinking water from E11 to P9. The dosage regimen was chosen on the basis of previous study [26] and has been previously shown to yield detectable concentrations of minocycline in the blood of adult mice and in the breast milk of lactating dams [27, 28]. Minocycline dosage was calculated based on body weight and drinking volume during pregnancy. To cover the taste of minocycline, sucrose (1%) was added to the solution. The water consumption was confirmed every day to make sure adequate drug delivery.

Statistical Analysis

Sample sizes were based on previous work of a similar nature by our laboratory [7, 20] and determined with power analysis (a two-tailed analysis with a significance set at $\alpha=0.05$ and power ≥ 80%) (G*Power software). No specific randomization method was used. Animals were randomly allocated into different experimental groups. All results are presented as means ± SEM and analyzed by the GraphPad Prism 6 software. Normality of data distribution was verified using the Shapiro–Wilk test. For Gaussian distribution, two-tailed unpaired Student's t test was used to compare differences between two independent groups. For non-Gaussian distribution, the Mann–Whitney U test was used to compare differences between two independent groups. The difference between multiple groups was calculated by two-way ANOVA followed by Bonferroni's post hoc analyses. Distributions of synaptic events were compared with Kolmogorov–Smirnov test. Differences were considered as significant at $p<0.05$.

Results

Generation of Cc2d1a cKO Mice

Earlier studies reported that *Cc2d1a* mRNA is expressed in the developing mouse cortex as early as E12.5 [8, 10], suggesting its possible role in cortical development. Here, we first conducted double immunofluorescent staining to determine the spatial expression patterns of CC2D1A protein in mouse embryonic brains at E14.5. CC2D1A protein is abundantly expressed in distinct cortical zones during embryonic development (Fig. 1a). We found almost all CC2D1A-positive cells in the intermediate zone (IZ) and ventricular zone (VZ) expressing neural stem/progenitor cell (NPC) marker nestin and immature neuronal marker doublecortin (DCX). To extend our analyses on the function of CC2D1A in neurodevelopment and brain function,

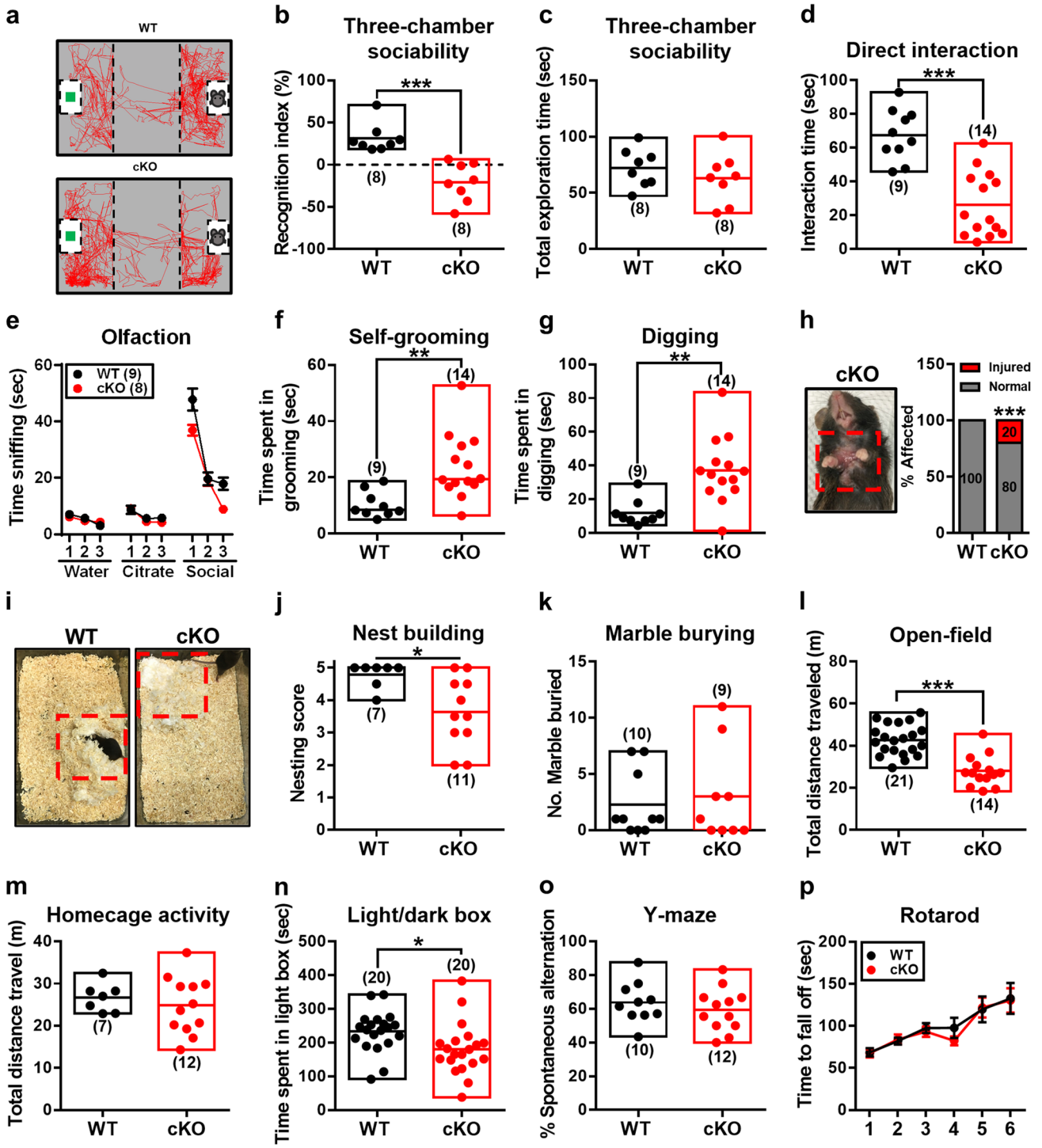

we generated cKO mice that show a loss of CC2D1A in neurons at an early stage of development by crossing the *Cc2d1a*$^{f/f}$ mice with *Emx*1-Cre mice (Fig. 1b). PCR screening of mouse genomic tail DNA confirmed heterozygous (*Cc2d1a*$^{f/+}$::*Emx-1*-Cre) and homozygous (*Cc2d1a*$^{f/f}$::*Emx1*-Cre) cKO mice (Fig. 1c). Immunoblots confirmed a reduction in CC2D1A protein expression in the forebrain at E14.5 and the mPFC at 8 weeks old in *Cc2d1a* cKO mice (Fig. 1d).

◂**Fig. 2** *Cc2d1a* cKO mice display autistic-like behaviors. **a** Representative movement traces of WT and cKO mice in the three-chamber sociability test. **b**, **c** Bar graph comparing the performance of WT and cKO mice on the recognition index ($t_{(14)}=5.15$, $p=0.0001$, $n=8$ in each group; two-tailed unpaired Student's t test) and the total exploration time ($t_{(14)}=0.93$, $p=0.37$, $n=8$ in each group; two-tailed unpaired Student's t test) in the three-chamber sociability test. **d** Bar graph comparing the performance of WT and cKO mice on direct social interaction test ($t_{(22)}=5.87$, $p<0.0001$; WT, $n=9$; cKO, $n=14$; two-tailed unpaired Student's t test). **e** Bar graph comparing the performance of WT and cKO mice on the olfactory habituation-dishabituation test. cKO mice showed unaltered ability to discriminate between orders (water, citrate, and social) and habituation to the same odor upon repeated presentation. cKO mice show a trend toward reduced time sniffing a social scent compared with WT mice, but did not reach statistically significance ($F_{(2,45)}=2.60$, $p=0.08$; WT, $n=9$; cKO, $n=18$; two-way ANOVA). **f**, **g** cKO mice spent significantly more time in repetitive behaviors, including self-grooming ($t_{(21)}=3.29$, $p=0.004$; two-tailed unpaired Student's t test) and digging ($t_{(21)}=3.74$, $p=0.001$; two-tailed unpaired Student`s t test) within a 10-min period in the home cage (WT, $n=9$; cKO, $n=14$). **h** Representative image and bar graph showing excessive abnormal grooming induced ulcerative dermatitis (red dashed boxed area) and the percentage of affected mice in a subset of cKO mice ($p<0.001$; WT, $n=0$ of 10; cKO, $n=2$ of 10; chi-square test). **i**, **j** Representative image and bar graph comparing the nest building performance of WT and cKO mice ($p=0.015$; WT, $n=7$; cKO, $n=11$; Mann–Whitney test). **k** Bar graph comparing the performance of WT and cKO mice on the marble burying test ($p>0.999$; WT, $n=10$; cKO, $n=9$; Mann–Whitney test). **l** Bar graph comparing the performance of WT and cKO mice on the total distance traveled in the open field during a 10-min test period ($t_{(33)}=5.87$, $p<0.0001$; WT, $n=21$; cKO, $n=14$; two-tailed unpaired Student's t test). **m** Bar graph comparing the performance of WT and cKO mice on the total distance traveled in the home cage ($t_{(17)}=0.66$, $p=0.52$; WT, $n=7$; cKO, $n=12$; two-tailed unpaired Student's t test). **n** Bar graph comparing the performance of WT and cKO mice on the time spent in the light compartment in the light/dark box test ($t_{(38)}=2.38$, $p=0.02$; WT, $n=20$; cKO, $n=20$; two-tailed unpaired Student's t test). **o** Bar graph comparing the performance of WT and cKO mice on the spontaneous alteration in the Y-maze test ($t_{(20)}=0.83$, $p=0.42$; WT, $n=10$; cKO, $n=12$; two-tailed unpaired Student's t test). **p** Bar graph comparing the performance of WT and cKO mice in the rotarod test ($F_{(5,108)}=0.21$, $p=0.96$; WT, $n=9$; cKO, $n=11$; two-way ANOVA). Data are represented as mean ± SEM. The total number of animal examined is indicated by n. $^{*}p<0.05$; $^{**}p<0.01$; $^{***}p<0.001$ compared with WT group

In comparison to WT embryos, no macroscopic malformations of *Cc2d1a* cKO embryos were found at E14.5 and E18.5 (Fig. 1e). *Cc2d1a* cKO newborn pups survived and displayed good general health. Total body weight did not differ between WT and cKO mice at P10 (Fig. 1f). The entire brain sizes of *Cc2d1a* cKO mice were not noticeably different from those of age-matched WT mice at E18.5 and P10 (Fig. 1g). We found no significance in the thickness of cortical plate and ventricular zone between WT and *Cc2d1a* cKO mice at E14.5 (Fig. 1h). As nestin-positive NPCs showed immunoreactivity for CC2D1A, we therefore examined whether CC2D1A deletion alters the proliferation of NPCs at E12.5 by using BrdU labeling. A significant reduction of the number of BrdU-positive cells was observed in *Cc2d1a* cKO mice (Fig. 1i). However, the radial migration of cortical neurons was not altered by CC2D1A deletion (Supplement Fig. 1a, b). To further determine the effect of CC2D1A deficiency on the laminar organization of cortical neurons, layer-specific markers, including the anti-Ctip2 antibody that labels deeper-layer neurons and the anti-Brn2 antibody that labels upper-layer neurons, were used. As shown in Fig. 1j, compared with those in WT mice, the number of Ctip2-positive cells in cortical layer V was significantly reduced in *Cc2d1a* cKO mice, whereas an increase in the number of Ctip2-positive cells was found in cortical layer VI in *Cc2d1a* cKO mice at P10. In 8-week-old WT mice, double immunofluorescent staining with the excitatory neurons neuronal marker CaMKIIα revealed that CC2D1A-expressing cells were co-labeled with CamkIIα in the mPFC. In cKO mice, we did not detect CC2D1A immunoreactivity in CamkIIα-expressing cells (Supplement Fig. 2a). In contrast, we did not detect CC2D1A immunoreactivity in glial cells, which were identified by antibody directed against the glial marker GFAP (Supplement Fig. 2a).

Cc2d1a cKO Mice Exhibit Autistic-Like Behaviors

Since our goal was to validate the role of CC2D1A deficiency in the genesis of autistic-like behaviors, two core behavioral features of ASD such as impaired social interactions and restricted repetitive behaviors were examined. We found that *Cc2d1a* cKO mice exhibited significantly reduced social interactions in the three-chamber social interaction test, showing diminished preference to investigate the social stimulus over the object without altering total exploration time (Fig. 2a–c). In addition, *Cc2d1a* cKO mice traveled less distance than WT mice (Supplement Fig. 3a). In the reciprocal social interaction test, *Cc2d1a* cKO mice displayed decreased sociability, with reduced time spent in reciprocal interactions with the novel stimulus mouse (Fig. 2d). To rule out the involvement of an olfactory deficit underlying social interaction deficits in *Cc2d1a* cKO mice, we performed the olfactory habituation-dishabituation test. *Cc2d1a* cKO mice demonstrated an intact ability to detect and discriminate between different odors but spent less time than WT mice sniffing a social odor, a feature consistent with a decreased interest in social stimuli (Fig. 2e). We next assessed restricted repetitive behaviors in *Cc2d1a* cKO mice. In comparison to WT mice, 8–12-week-old *Cc2d1a* cKO mice spend more time engaged in stereotypical behaviors such as self-grooming (Fig. 2f) and digging (Fig. 2g).

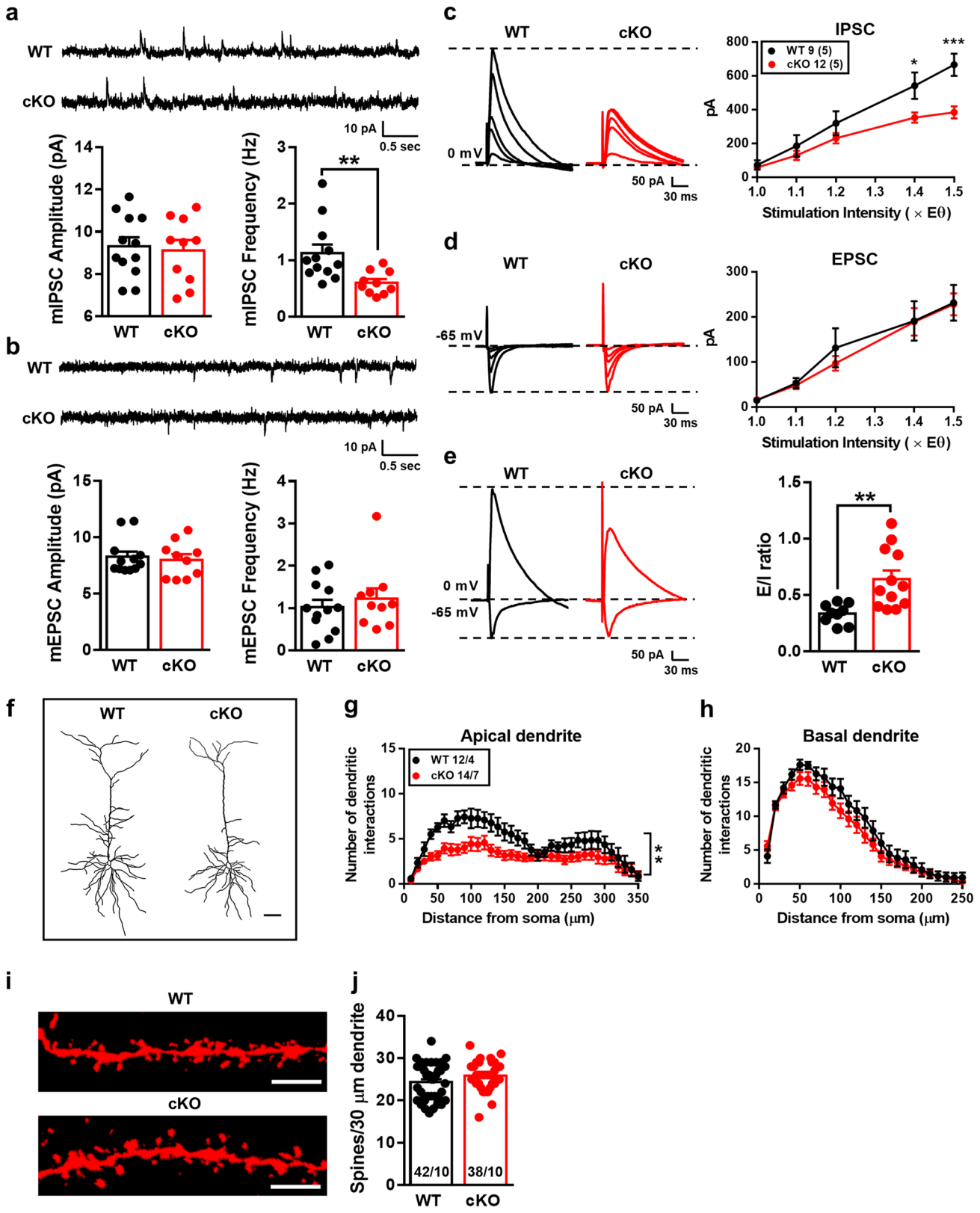
a
WT
cKO
10 pA
0.5 sec
mIPSC Amplitude (pA)
mIPSC Frequency (Hz)
**
WT
cKO
b
WT
cKO
10 pA
0.5 sec
mEPSC Amplitude (pA)
mEPSC Frequency (Hz)
WT
cKO
c
WT
cKO
0 mV
50 pA
30 ms
IPSC
WT 9 (5)
cKO 12 (5)
*
***
pA
Stimulation Intensity (× Eθ)
d
WT
cKO
-65 mV
50 pA
30 ms
EPSC
pA
Stimulation Intensity (× Eθ)
e
WT
cKO
0 mV
-65 mV
50 pA
30 ms
E/I ratio
**
WT
cKO
f
WT
cKO
g
Apical dendrite
WT 12/4
cKO 14/7
Number of dendritic interactions
**
Distance from soma (μm)
h
Basal dendrite
Number of dendritic interactions
Distance from soma (μm)
i
WT
cKO
j
Spines/30 μm dendrite
42/10
38/10
WT
cKO

◂**Fig. 3** CC2D1A deletion results in aberrant dendritic morphology and synaptic transmission in mPFC pyramidal neurons. **a** Representative traces of mIPSCs and bar graph comparing the amplitude ($t_{(20)}=0.30$, $p=0.76$; WT, $n=12$ neurons from 4 mice; cKO, $n=10$ neurons from 4 mice; two-tailed unpaired Student's t test) and frequency ($t_{(20)}=2.97$, $p=0.007$; WT, $n=12$ neurons from 4 mice; cKO, $n=10$ neurons from 4 mice; two-tailed unpaired Student's t test) of mEPSCs in layer V pyramidal neurons from WT and cKO mice. **b** Representative traces of mEPSCs and bar graph comparing the amplitude ($t_{(20)}=0.42$, $p=0.67$; WT, $n=12$ neurons from 4 mice; cKO, $n=10$ neurons from 4 mice; two-tailed unpaired Student's t test) and frequency ($t_{(20)}=0.69$, $p=0.49$; WT, $n=12$ neurons from 4 mice; cKO, $n=10$ neurons from 4 mice; two-tailed unpaired Student's t test) of mIPSCs in layer V pyramidal neurons from WT and cKO mice. **c** Representative traces and input–output relationships for IPSCs in slices from WT and cKO mice (group × stimulus intensity: $F_{(4,95)}=2.85$, $p=0.02$; WT: $n=9$ neurons from 5 mice; cKO: $n=12$ neurons from 5 mice; two-way repeated-measures ANOVA). $^{*}p<0.05$, compared with WT group (two-way ANOVA followed by Bonferroni's post hoc analyses). $^{***}p<0.001$, compared with WT group (two-way ANOVA followed by Bonferroni's post hoc analyses). **d** Representative traces and input–output relationships for EPSCs in slices from WT and cKO mice (group × stimulus intensity: $F_{(4,95)}=0.16$, $p=0.95$; WT: $n=9$ neurons from 5 mice; cKO: $n=12$ neurons from 5 mice; two-way repeated-measures ANOVA). **e** Representative traces and the E/I ratio recorded in slices from WT and cKO mice. The E/I ratios were calculated by dividing the amplitudes of EPSCs by the amplitudes of IPSCs from the same cell recorded at the same stimulation intensity ($t_{(19)}=3.31$, $p=0.003$; two-tailed unpaired Student's t test). **f** Representative camera lucida tracings of mPFC layer V pyramidal neurons from WT and cKO mice. Scale bar, 50 µm. **g**, **h** Sholl analysis of apical ($F_{(41,1008)}=1.83$, $p=0.0012$; two-way repeated-measures ANOVA) and basal ($F_{(41,1008)}=0.86$, $p=0.73$; two-way repeated-measures ANOVA) dendrites of mPFC layer V pyramidal neuron from WT (12 neurons from 4 mice) and cKO (14 neurons from 7 mice). **i** Representative images of biocytin-labeled secondary apical dendrites of mPFC layer V pyramidal neurons from WT and cKO mice. Scale bar, 10 µm. **j** Summary bar graph depicting the density of protrusions in apical dendrites of layer V pyramidal neuron ($t_{(73)}=1.63$, $p=0.11$; two-tailed unpaired Student's t test) from WT (42 neurons from 10 mice) and cKO mice (38 neurons from 10 mice). Data are represented as mean ± SEM. $^{**}p<0.01$ compared with WT group

Notably, by the age of 4–6 months, cKO mice developed pronounced skin lesions on the back of the neck (2 of 10, 20%) (Fig. 2h). No skin lesions were observed in WT mice (0 of 10). Additionally, *Cc2d1a* cKO mice displayed lower nesting scores in the nest building test (Fig. 2i, j), based on Deacon's method [24]. However, in the marble-burying test, an assay of repetitive and compulsive-like behaviors, *Cc2d1a* cKO mice buried approximately the same number of marbles as WT mice (Fig. 2k).

Given that anxiety disorders have also been noted in youth with ASD [29], we thus examined whether CC2D1A deletion may alter anxiety-like behavior. In the open-field test, *Cc2d1a* cKO mice traveled less distance than WT mice (Fig. 2l), while a percentage of time spent in the central zone was unchanged (Supplement Fig. 3b). Impaired locomotor activity is unique to novel environments because *Cc2d1a* cKO mice displayed normal locomotor activity in their home cage, a familiar environment (Fig. 2m). In the light/dark box test, *Cc2d1a* cKO mice spent significantly less time in the light box (Fig. 2n) an increased latency to enter the light box (Supplement Fig. 3c) compared with those in WT mice. In addition, *Cc2d1a* cKO mice showed no impairment in spontaneous alternation behavior in the Y-maze (Fig. 2o), suggesting intact cognitive flexibility. There was no significant difference in the latency to fall between WT and *Cc2d1a* cKO mice in the rotarod test (Fig. 2p), indicating normal motor coordination function.

CC2D1A Deletion Alters Dendritic Morphology and Synaptic Transmission in the mPFC of Adult Brain

The mPFC is a crucial brain region implicated in mediating autistic-like behaviors [30–33]. Given that an altered cortical excitation-inhibition balance has been implicated in ASD pathology [34, 35], we next examined whether CC2D1A deletion alters the E/I ratio in mPFC layer V pyramidal neurons (Supplement Fig. 4a). We found that the frequency but not amplitude of mIPSC was significantly lower in pyramidal neurons from *Cc2d1a* cKO mice (Fig. 3a and Supplement Fig. 4b, c). No difference was found between groups in the frequency and amplitude of mEPSC (Fig. 3b and Supplement Fig. 4d, e). Furthermore, the amplitude of evoked IPSC (Fig. 3c) but not EPSCs (Fig. 3d) was significantly smaller in pyramidal neurons from *Cc2d1a* cKO mice than those from WT mice. *Cc2d1a* cKO mice display a significantly higher E/I ratio than WT mice (Fig. 3e). To investigate whether CC2D1A deletion may influence dendritic geometry and spine density, we used biocytin labeling to visualize individual neurons (Fig. 3f) and analyzed the complexity of their dendritic arborization. Sholl analysis of reconstructed mPFC layer V pyramidal neurons revealed that CC2D1A deletion significantly decreased the complexity of apical (Fig. 3g) but not basal dendrite branching (Fig. 3h). No significant changes in the density of dendritic protrusions were detected on secondary and tertiary branches of apical dendrites of mPFC layer V pyramidal neurons in *Cc2d1a* cKO mice (Fig. 3i, j).

Minocycline Treatment Rescues Autistic-Like Features in Cc2d1a cKO Mice

We next sought to determine whether autistic-like features associated with CC2D1A deficiency could be rescued during early development. Minocycline, a tetracycline antibiotic,

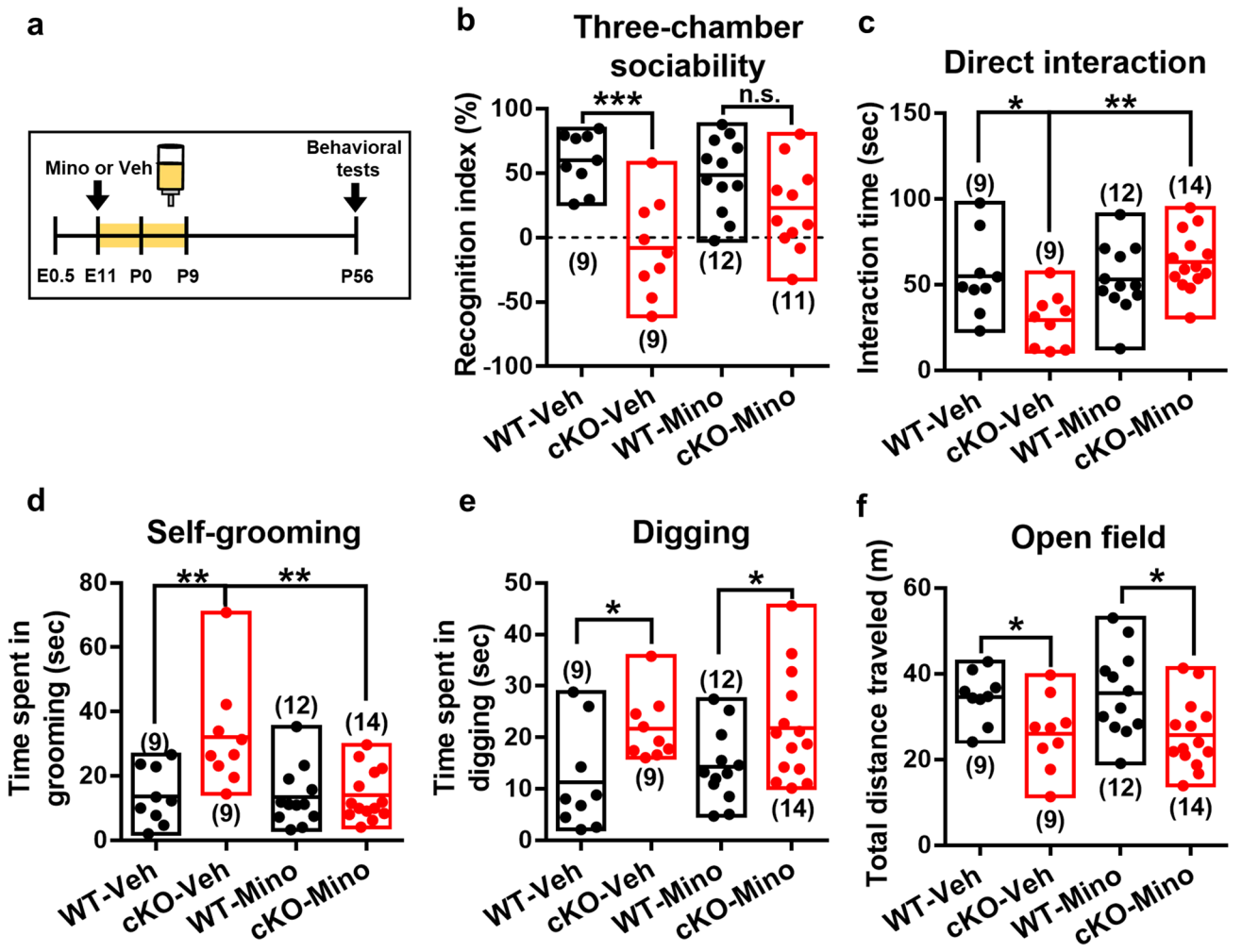

Fig. 4 Treatment with minocycline ameliorates autistic-like behavior in *Cc2d1a* cKO mice. **a** Schematic illustration of the experimental design. Minocycline (30 mg/kg) was administered from E11-P9 by adding it to the drinking water of the dam, and the behavioral tests were carried out after P56. **b** Bar graph comparing the performance of WT and cKO mice with Veh or Mino treatment on the recognition index in the three-chamber sociability test. Two-way ANOVA revealed effects of cKO ($F_{(1,37)}=22.95$, $p<0.001$), minocycline treatment ($F_{(1,37)}=0.97$, $p=0.33$), and cKO × minocycline treatment interaction ($F_{(1,37)}=4.61$, $p=0.038$, $n=9$–12 in each group). **c** Bar graph comparing the performance of WT and cKO mice with vehicle (Veh) or minocycline (Mino) treatment on direct social interaction test. Two-way ANOVA revealed effects of cKO ($F_{(1,40)}=1.684$, $p=0.202$), minocycline treatment ($F_{(1,40)}=7.44$, $p=0.009$) and cKO × minocycline treatment interaction ($F_{(1,40)}=9.278$, $p=0.004$, $n=9$–14 in each group). **d** Bar graph comparing the performance of WT and cKO mice with Veh or Mino treatment on self-grooming behavior within a 10-min period in the home cage. Two-way ANOVA revealed effects of cKO ($F_{(1,40)}=8.295$, $p=0.006$), minocycline treatment ($F_{(1,40)}=7.915$, $p=0.008$) and cKO × minocycline treatment interaction ($F_{(1,40)}=7.378$, $p=0.01$, $n=9$–14 in each group). **e** Bar graph comparing the performance of WT and cKO mice with Veh or Mino treatment on digging behavior within a 10-min period in the home cage. Two-way ANOVA revealed effects of cKO ($F_{(1,40)}=10.97$, $p=0.002$), minocycline treatment ($F_{(1,40)}=0.298$, $p=0.588$), and cKO × minocycline treatment interaction ($F_{(1,40)}=0.283$, $p=0.598$, $n=9$–14 in each group). **f** Bar graph comparing the performance of WT and cKO mice with Veh or Mino treatment on the total distance traveled in the open field during a 10-min test period. Two-way ANOVA revealed effects of cKO ($F_{(1,40)}=12.39$, $p=0.001$), minocycline treatment ($F_{(1,40)}=0.011$, $p=0.916$), and cKO × minocycline treatment interaction ($F_{(1,40)}=0.052$, $p=0.821$, $n=9$–14 in each group). Data are represented as mean ± SEM. The total number of animal examined is indicated by *n*. $*p<0.05$; $**p<0.01$; $***p<0.001$ compared with WT-Veh, cKO-Veh or WT-Mino group. n.s., not significant (two-way ANOVA followed by Bonferroni`s post hoc analyses)

has been found effective as an adjunct drug in improving many different mental disorders, including depression [36], bipolar disorder [37], schizophrenia [38], and ASD [39]. Interestingly, minocycline administration during the first postnatal week was shown to effectively restore the abnormal wiring in prefrontal circuits and cognitive deficits in dual-hit genetic-environmental mice [40]. These findings prompted us to examine whether early postnatal minocycline treatment may rescue autistic-like features observed in *Cc2d1a* cKO mice. We administrated minocycline from

E11 to P9 by adding to the drinking water of the dam [26, 40] and analyzed the morphological, functional, and behavioral consequences in adulthood (Fig. 4a). We observed that minocycline administration rescued social interaction deficits in *Cc2d1a* cKO mice, significantly increasing the time spent by *Cc2d1a* cKO mice in social interactions in both the three-chamber sociability test (Fig. 4b) and reciprocal social interaction test (Fig. 4c). Consistently, minocycline administration mitigated stereotypic repetitive behaviors in *Cc2d1a* cKO mice as indicated by a significant reduction of the total times spent in self-grooming (Fig. 4d). However, the total times spent in digging and the hypoactivity in the open-field test in *Cc2d1a* cKO mice were not rescued by minocycline treatment (Fig. 4e, f).

We also elucidated whether minocycline mitigated autistic-like behaviors in *Cc2d1a* cKO mice by restoring the abnormalities in synaptic transmission and dendritic complexity of mPFC layer V pyramidal neurons. We found that minocycline was sufficient to normalize E/I ratio in *Cc2d1a* cKO mice (Fig. 5a, b). Similarly, minocycline treatment rescued the decrease of mIPSC frequency in pyramidal neurons from *Cc2d1a* cKO mice compared with vehicle-treated group (Fig. 5c). There was no statistically significant difference between groups with respect to the frequency and amplitude of mEPSC (Fig. 5d). We also observed that minocycline administration effectively rescued the defective dendritic complexity in mPFC layer V pyramidal neurons of *Cc2d1a* KO mice (Fig. 5e). Sholl analysis of reconstructed mPFC layer V pyramidal neurons revealed no significant differences between minocycline-treated WT and *Cc2d1a* cKO mice in the complexity of both apical (Fig. 5f) and basal dendrite branching (Fig. 5g). Moreover, minocycline treatment rescued the altered laminar organization of cortical neurons observed in *Cc2d1a* cKO mice at P10. There was no significant difference between minocycline-treated WT and *Cc2d1a* cKO mice in the thickness of the cortical plate (layers I-VI) (Fig. 5h).

Discussion

ASD is associated with heterogeneous genetic variations, and more than 100 candidate genes and genetic variants have been implicated in ASD [41]. While associations of loss-of-function mutations in the human *Cc2d1a* gene with ASD have been reported previously [8, 10, 11], the pathogenic origin of the autistic-like features of CC2D1A deficiency remains unclear. Progress has been hampered by the lack of appropriate animal models that fully recapitulate the core symptoms of ASD. In this study, we created a novel mouse model to study the role of CC2D1A and found that CC2D1A deletion leads to autistic-like features characterized by reduced social interactions, increased stereotypic repetitive behaviors, and altered synaptic structure and function in the mPFC. More importantly, we demonstrate direct evidence that minocycline administration during the embryonic and early postnatal periods can effectively rescue both behavioral and synaptic abnormalities observed in *Cc2d1a* cKO mice.

Our data are consistent with CC2D1A protein being strongly expressed in embryonic mouse cortices. CC2D1A protein is expressed in NPCs in the embryonic forebrain to control cell proliferation. Given that *Cc2d1a* null mice die shortly after birth owing to respiratory distress [4, 12], Cre-loxP technology was used to generate *Cc2d1a* cKO mice. For example, it has been reported that *Cc2d1a* ablation in postnatal forebrain using *Camk2α*-Cre line resulted in cognitive and social impairments [7, 13]. While some autistic-like behaviors were detected in *Camk2α*-Cre-mediated cKO mice [13], we wondered whether more severe behavioral disturbances are detectable in mice with conditional ablation of *Cc2d1a* at early embryonic time point. Although both *Nestin*-Cre and *Emx1*-Cre lines are useful for conditional ablation of LoxP-flanked target genes during embryonic development, we chose *Emx1*-Cre line to generate *Cc2d1a* cKO mice. This is due to mice with *Cc2d1a* ablation using the *Nestin*-Cre line died after birth [13, 42]. *Emx1*-Cre-mediated cKO mice are fertile, viable, and have normal brain anatomical features and body weight. In line with findings of ASD in human patients with loss-of-function mutations in CC2D1A, *Cc2d1a* cKO mice displayed significantly increased repetitive self-grooming and digging, as well as aberrant social interactions in both the three-chamber social interaction test and reciprocal social interaction test. *Cc2d1a* cKO mice were able to discriminate between different odors in the olfactory habituation-dishabituation test, indicating that their olfactory system was functional, but showed a significant decrease in time spent sniffing the social odor. These behavioral phenotypes have been described across a number of genetic mouse ASD models, including *Shank2* [43, 44], *Shank3* [45, 46], *phosphatase and tensin homolog on chromosome ten* [*Pten*; 47, 48], *fragile X mental retardation 1* [*Fmr1*; 49, 19], *cyclin-dependent kinase-like 5* [*Cdkl5*; 23], and *contactin-associated protein-like 2* [*CNTNAP2*; 33]. Compared to *Camk2α*-Cre-mediated cKO mice, some autistic-like phenotypes (e.g., aberrant social interactions in the three-chamber sociability test and reciprocal social interaction test, and excessive repetitive grooming) were consistently observed for both *Camk2α*-Cre and *Emx1*-Cre *Cc2d1a* cKO mice (Table 1). Additionally, *Emx1*-Cre *Cc2d1a* cKO mice cKO mice traveled less distance in the open-field test but exhibited increased anxiety-like behavior in the light/dark box test. These additional phenotypes may be mediated by conditional ablation of *Cc2d1a* at early embryonic stages.

Marble-burying in rodents is often used as an index for the repetitive and compulsive-like behaviors in humans [50, 51]. Previous studies have shown that several genetic mouse models of ASD built by loss of *Shank3* [52, 53], *Pten* [54],

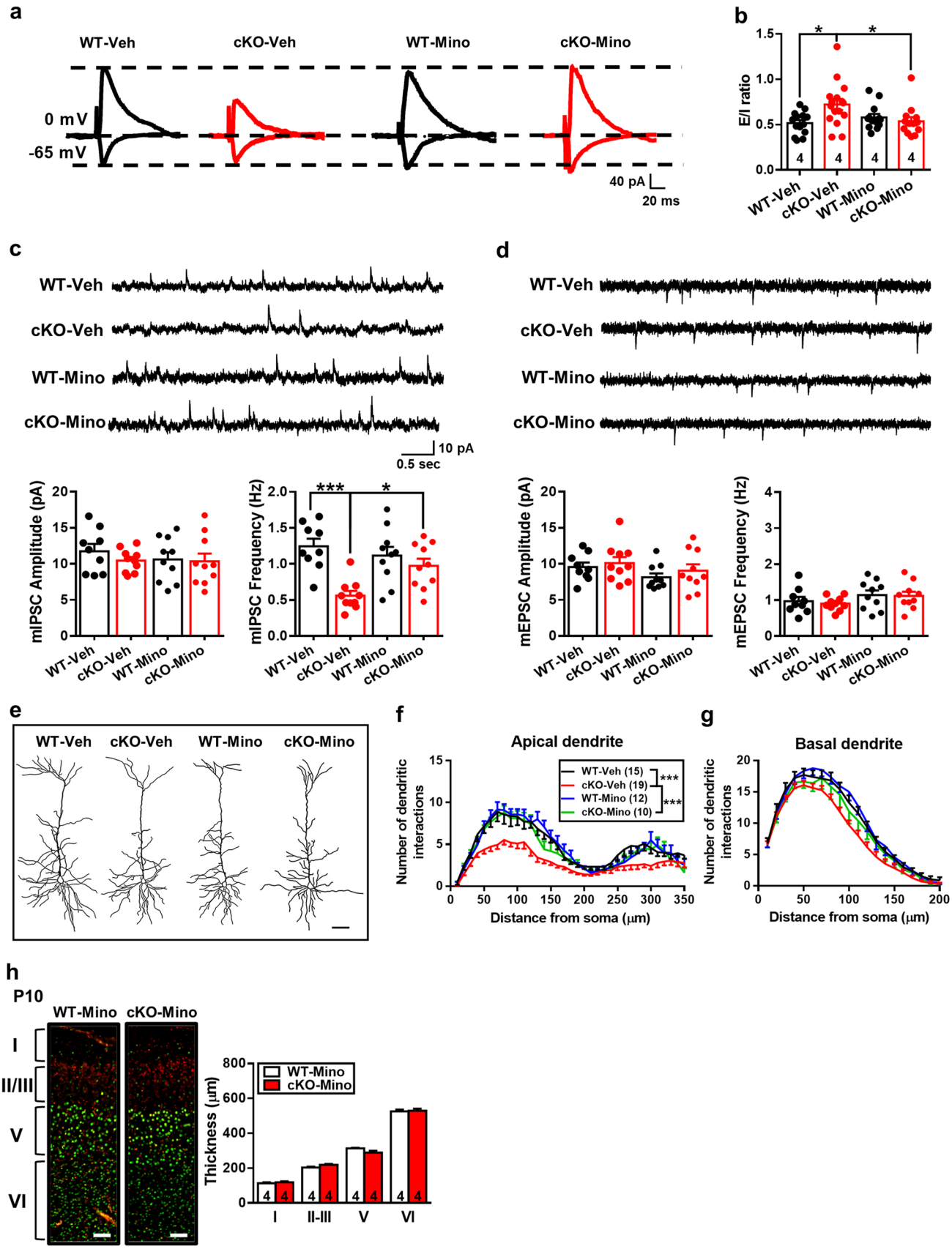
a
WT-Veh
cKO-Veh
WT-Mino
cKO-Mino
0 mV
-65 mV
40 pA
20 ms
b
E/I ratio
WT-Veh
cKO-Veh
WT-Mino
cKO-Mino
c
10 pA
0.5 sec
mIPSC Amplitude (pA)
mIPSC Frequency (Hz)
d
mEPSC Amplitude (pA)
mEPSC Frequency (Hz)
e
f
Apical dendrite
WT-Veh (15)
cKO-Veh (19)
WT-Mino (12)
cKO-Mino (10)
Number of dendritic interactions
Distance from soma (μm)
g
Basal dendrite
h
P10
I
II/III
V
VI
Thickness (μm)

◂**Fig. 5** Minocycline treatment restores aberrant morphology and synaptic function in *Cc2d1a* cKO mice. **a**, **b** Representative traces and the E/I ratio recorded in mPFC layer V pyramidal neurons from WT and cKO mice with vehicle or minocycline treatment. Two-way ANOVA revealed effects of cKO ($F_{(1,52)}=2.86$, $p=0.10$), minocycline treatment ($F_{(1,52)}=1.62$, $p=0.21$), and cKO×minocycline treatment interaction ($F_{(1,52)}=6.66$, $p=0.01$). Post hoc analysis revealed that minocycline treatment significantly rescues the increased E/I ratio in cKO mice ($p<0.05$). **c** Representative traces of mIPSCs and bar graph comparing the amplitude and frequency from WT and cKO mice with vehicle or minocycline treatment. Amplitude: Two-way ANOVA revealed effects of cKO ($F_{(1,35)}=0.739$, $p=0.577$), minocycline treatment ($F_{(1,35)}=0.452$, $p=0.506$), and cKO×minocycline treatment interaction ($F_{(1,35)}=0.317$, $p=0.577$). Frequency: Two-way ANOVA revealed effects of cKO ($F_{(1,35)}=16.93$, $p<0.001$), minocycline treatment ($F_{(1,35)}=1.997$, $p=0.166$), and cKO×minocycline treatment interaction ($F_{(1,35)}=7.283$, $p=0.01$; WT-Veh: $n=9$ neurons from 2 mice; cKO-Veh: $n=10$ neurons from 4 mice; WT-Mino: $n=10$ neurons from 3 mice; cKO-Mino: $n=10$ neurons from 3 mice). Post hoc analysis revealed that minocycline treatment significantly rescues the decreased mIPSC frequency in cKO mice ($p<0.05$). **d** Representative traces of mEPSCs and bar graph comparing the amplitude and frequency from WT and cKO mice with vehicle or minocycline treatment. Amplitude: Two-way ANOVA revealed effects of cKO ($F_{(1,35)}=0.999$, $p=0.324$), minocycline treatment ($F_{(1,35)}=2.787$, $p=0.104$), and cKO×minocycline treatment interaction ($F_{(1,35)}=0.065$, $p=0.799$). Frequency: Two-way ANOVA revealed effects of cKO ($F_{(1,35)}=0.176$, $p=0.677$), minocycline treatment ($F_{(1,35)}=3.087$, $p=0.087$), and cKO×minocycline treatment interaction ($F_{(1,35)}=0.041$, $p=0.839$; WT-Veh: $n=9$ neurons from 2 mice; cKO-Veh: $n=10$ neurons from 4 mice; WT-Mino: $n=10$ neurons from 3 mice; cKO-Mino: $n=10$ neurons from 3 mice). **e** Representative camera lucida tracings of mPFC layer V pyramidal neurons from WT and cKO mice with vehicle or minocycline treatment. Scale bar, 50 µm. **f**, **g** Sholl analysis of apical and basal dendrites of mPFC layer V pyramidal neuron from WT-Veh (15 neurons from 4 mice), cKO-Veh (19 neurons from 7 mice), WT-Mino (12 neurons from 4 mice), and cKO-Mino mice (10 neurons from 5 mice). Minocycline treatment significantly rescues the reduced complexity of apical dendrites of mPFC layer V pyramidal neurons in cKO mice ($F_{(49,1350)}=4.38$, $p<0.0001$; two-way repeated measures ANOVA). **h** Representative double immunofluorescence staining for Ctip2 (layer V and VI marker; green) and Brn2 (layer II–III and V marker; red) in cerebral cortices from WT-Mino and cKO-Mino mice at P10. Scale bar, 100 µm. The total number of animal examined is indicated by *n*. *$p<0.05$; ***$p<0.001$ compared with WT-Veh, cKO-Veh or WT-Mino group

or *Fmr1* [55] bury significantly fewer marbles than control mice in the marble-burying test. However, *Cc2d1a* cKO mice displayed normal marble-burying activity. Consistently, the lack of effect of CC2D1A deletion in marble-burying behavior was also observed in *Camk2α*-Cre-mediated cKO mice [13]. One possible explanation is that mutations in different ASD risk genes may lead to varying degrees of severity in ASD-related behavioral phenotypes. In addition, we noticed that *Cc2d1a* cKO mice displayed decreased total distance traveled in the open-field test. As the percentage of time spent in the central zone remained unaltered in *Cc2d1a* cKO mice, the reduction of locomotor activity could not be explained by a reduction of anxiety-like behavior. The abnormal locomotor activity of *Cc2d1a* cKO mice is limited to the exposure to novel environment because they displayed normal locomotor activity in the familiar environment of their home cage.

One long-standing proposed mechanism for the development of ASD is the disruption of E/I balance in key cortical and subcortical neural circuits [35, 56, 57]. There is still no consensus on whether the E/I balance is biased toward excitation or inhibition in ASD-related neural circuits. A recent study for a systematic test of the E/I balance hypothesis across four genetically distinct ASD mouse models (*Fmr1*$^{-/y}$, *Cntnap2*$^{-/-}$, *16p11.2*$^{del/+}$, *Tsc2*$^{+/-}$) suggests that elevated E/I ratio in somatosensory cortex is a common circuit phenotype in ASD mice [33]. Although a greater decrease in inhibition than excitation is associated with elevated E/I ratio observed in these transgenic ASD mouse models, it does not exclude the possibility that genetically distinct forms of ASD may affect E/I ratio in different ways [57, 58]. Our result corroborates previous studies showing that an elevated E/I ratio in the mPFC leads to social behavior deficits in WT and *CNTNAP2* cKO mice [33, 59]. *Cc2d1a* cKO mice exhibited significantly elevated E/I ratio due to a reduction of GABAergic transmission. *Cc2d1a*

Table 1 Phenotypes of *Cc2d1a*conditional knockout mice

Measurements	Behavioral tests	Mouse models	
		CamkIIα-Cc2d1a	*Emx-1-Cc2d1a*
Social function	Reciprocal social interaction tests	↓	↓
	Three-chamber sociability test	↓	↓
	Nesting test	n.a	↓
Repetitive behaviors	Digging	↓	↑
	Grooming	↑	↑
Anxiety-like behaviors	Open-field test (locomotion)	↑Anxiety-like	↓
	Open-field test (time in central zone)	↓Anxiety-like	n.s
	Light/dark box test	n.a	↑Anxiety-like
	Marble burying test	n.s	n.s

Targeting *Cc2d1a*deletion by different Cre lines (*CamkIIα*and *Emx-1*) recapitulated different subsets of behavioral phenotypes. ↑ indicates an increase, ↓ indicates a decrease, n.s. indicates not significant, and n.a. indicates not applicable, as the experiment was not conducted. The results of *CamkIIα-Cc2d1a*mice were obtained from Oaks et al. [13]

cKO mice showed reduction in the frequency but not amplitude of mIPSC, suggesting that a major consequence of CC2D1A deletion is a downregulation of GABAergic innervation of layer V mPFC pyramidal neurons. A similar reduction in mIPSC frequency was also observed in *Cc2d1a*-deficient cortical primary neuronal cultures [9]. Nevertheless, more studies are needed to validate how CC2D1A controls the maturation of GABAergic synapses onto layer V pyramidal neurons in the mPFC. However, we could not exclude the possibility that CC2D1A may indirectly modulate GABAergic transmission onto mPFC pyramidal neurons through a retrograde regulatory mechanism. Regardless of the mechanism of action of CC2D1A deletion, these observations beg the question of how E/I imbalance contributes to the emergence of autistic-like behaviors. The E/I balance has been firmly established in playing a critical role in controlling excitability, input gating, and dynamic range expansion in neural circuits, which all may make contribution to the pathogenic mechanisms underlying the symptoms of ASD due to E/I imbalance [57, 58]. Abnormal dendrite and spine morphology of cortical neurons has been observed in ASD patients and several mouse models of ASD [60–63]. Consistently, our morphometric analysis revealed significant reduction in apical dendritic complexity of mPFC pyramidal neurons in *Cc2d1a* cKO mice. However, we did not observe a significant change in spine density on mPFC pyramidal neuron dendrites in *Cc2d1a* cKO mice. This is similar to what has been observed in *Camk2α*-Cre-mediated *Cc2d1a* cKO mice where CC2D1A deletion did not alter spine density in apical dendrites of CA1 pyramidal neurons [7]. Therefore, it is possible that CC2D1A has distinct roles in the regulation of dendritic morphology and spine maintenance. Further investigation is required to establish causality between neuronal morphology alterations and the development of autistic-like phenotypes.

Minocycline has been shown to exert its neuroprotective effects in numerous neurological disorders [64]. Although results from a small pilot study revealed no clinical improvement in children with regressive autism after minocycline treatment [65], a recent randomized placebo-controlled trial showed that it is an effective adjuvant to risperidone for improvement of irritability and hyperactivity symptoms in ASD children [39]. Here, we extend these clinical findings and demonstrate the efficacy of minocycline in ameliorating autistic-like behavioral and synaptic abnormalities observed in *Cc2d1a* cKO mice. The underlying mechanisms behind phenotypic rescue remain to be investigated. Given that minocycline possesses potent anti-inflammatory activity [66, 67], it will therefore be interesting to determine whether these effects are mediated through suppressing microglial activation and pro-inflammatory cytokine production. Indeed, evidence indicates that autistic children suffer from ongoing neuroinflammation throughout the brain involving microglial activation [68–70]. There is also some evidence to suggest that minocycline can enhance GABAergic synaptic transmission [71], alter synaptic protein expression [72], and improve neuronal structures [17]. Since *Cc2d1a* cKO mice display reduced dendritic complexity and a decrease in synaptic GABAergic transmission, further studies are warranted to evaluate whether chronic minocycline treatment improves autistic-like behaviors in *Cc2d1a* cKO mice by restoring neuronal structures and synaptic function.

The molecular mechanisms by which *Cc2d1a* knockdown leads to synaptic and behavioral abnormalities remain largely unresolved. Because our previous study showed that Rac1 hyperactivity consequent to the loss of CC2D1A results in impairments of hippocampal synaptic plasticity and cognitive dysfunction [7], it is possible that excessive Rac1 function may also lead to autistic-like phenotypes. Indeed, Rac1 has been identified as a converging factor downstream of numerous proteins encoded by ASD risk genes, such as *Shank3* [73], *Fmr1* [74], and *Dock4* [75], revealing a critical role for Rac1 activity in ASD pathophysiology. In addition, our findings should also be interpreted with caution due to the use of only males for test subjects.

In conclusion, our results uncover a critical role for CC2D1A signaling in regulating prefrontal cortical development and function. We suggest that embryonic CC2D1A ablation initiates the pathological cascades leading to an elevated E/I ratio but a reduced morphological complexity in layer V mPFC pyramidal neurons, ultimately resulting in the emergence of numerous autistic-like behaviors including self-injurious repetitive grooming and aberrant social interactions. In a novel disease model of ASD, we show that minocycline can effectively rescue both behavioral and synaptic abnormalities, supporting a therapeutic potential of minocycline for treating autistic-like phenotypes caused by loss-of-function mutations in CC2D1A.

Supplementary Information The online version contains supplementary material available at https://doi.org/10.1007/s13311-021-01072-z.

Required Author Forms Disclosure forms provided by the authors are available with the online version of this article.

Author Contribution CYY, YCH, KHC, PL, and KSH designed research; CYY, YCH, and KHC performed research; CYY, YCH, and KHC analyzed data; PL provided *Cc2d1a*$^{f/f}$ mice; CYY, PL, and KSH wrote the paper.

Funding This work was supported by research grants from the National Health Research Institute (NHRI-EX108-10613NI; NHRI-EX109-10912NI; NHRI-EX110-10912NI) and the Ministry of Science and Technology (107–2320-B-006–037-MY3; 108–2321-B-006–025-MY2; 109–2320-B-006 -039 -MY3), Taiwan.

Declarations

Conflict of Interest The authors declare no competing interests.

References

1. Matsuda A, Suzuki Y, Honda G, Muramatsu S, Matsuzaki O, Nagano Y, et al. Large-scale identification and characterization of human genes that activate NF-κB and MAPK signaling pathways. Oncogene. 2003;22:3307-3318.
2. Shi ZY, Li YJ, Zhang KJ, Gao XC, Zheng ZJ, Han N, et al. Positive association of CC2D1A and CC2D2A gene haplotypes with mental retardation in a Han Chinese population. DNA Cell Biol. 2012;31:80-87.
3. Nakamura A, Naito M, Tsuruo T, Fujita N. Freud-1/Aki1, a novel PDK1-interacting protein, functions as a scaffold to activate the PDK1/Akt pathway in epidermal growth factor signaling. Mol Cell Biol. 2008;28:5996-6009.
4. Al-Tawashi A, Jung SY, Liu D, Su B, Qin J. Protein implicated in nonsyndromic mental retardation regulates protein kinase A activity. J Biol Chem. 2012;287:14644-14658.
5. Al-Tawashi A, Gehring C. Phosphodiesterase activity is regulated by CC2D1A that is implicated in non-syndromic intellectual disability. Cell Commun Signal. 2013;11:47.
6. Zamarbide M, Mossa A, Munõz-Llancao P, Wilkinson MK, Pond HL, Oaks AW, et al. Male-specific cAMP signaling in the hippocampus controls spatial memory deficits in a mouse model of autism and intellectual disability. Biol Psychiatry. 2019;85:760-768.
7. Yang CY, Yu TH, Wen WL, Ling P, Hsu KS. Conditional deletion of CC2D1A reduces hippocampal synaptic plasticity impairs cognitive function through Rac1 hyperactivation. J Neurosci. 2019;39:4959-4975.
8. Basel-Vanagaite L, Attia R, Yahav M, Ferland RJ, Anteki L, Walsh CA, et al. The CC2D1A, a member of a new gene family with C2 domains, is involved in autosomal recessive non-syndromic mental retardation. J Med Genet. 2006;43:203-210.
9. Zhao M, Raingo J, Chen ZJ, Kavalali ET. Cc2d1a, a C2 domain containing protein linked to nonsyndromic mental retardation, controls functional maturation of central synapses. J Neurophysiol. 2011;105:1506-1515.
10. Manzini MC, Xiong L, Shaheen R, Tambunan DE, Di Costanzo S, Mitisalis V, et al. CC2D1A regulates human intellectual and social function as well as NF-κB signaling homeostasis. Cell Rep. 2014;8:647-655.
11. Sener EF, Cıkılı Uytun M, Korkmaz Bayramov K, Zararsiz G, Oztop DB, Canatan H, et al. The roles of CC2D1A and HTR1A gene expressions in autism spectrum disorders. Metab Brain Dis. 2016;31:613-619.
12. Chen KR, Chang CH, Huang CY, Lin CY, Lin WY, Lo YC, et al. TBK1-associated protein in endolysosomes (TAPE)/CC2D1A is a key regulator linking RIG-I-like receptors to antiviral immunity. J Biol Chem. 2012;287:32216-32221.
13. Oaks AW, Zamarbide M, Tambunan DE, Santini E, Di Costanzo S, Pond HL, et al. *Cc2d1a* loss of function disrupts functional and morphological development in forebrain neurons leading to cognitive and social deficits. Cereb Cortex. 2017;27:1670-1685.
14. Zamarbide M, Oaks AW, Pond HL, Adelman JS, Manzini MC. Loss of the intellectual disability and Autism gene Cc2d1a and its homolog Cc2d1b differentially affect spatial memory, anxiety, and hyperactivity. Front Genet. 2018;9:65.
15. Richardson L , Venkataraman S, Stevenson P, Yang Y, Moss J, Graham L, et al. EMAGE mouse embryo spatial gene expression database: 2014 update. Nucleic Acids Res. 2014;42:D835-D844.
16. Gorski JA, Talley T, Qiu M, Puelles L, Rubenstein JL, Jones KR. Cortical excitatory neurons and glia, but not GABAergic neurons, are produced in the Emx1-expressing lineage. J Neurosci. 2002;22:6309-6314.
17. Yau SY, Bettio L, Vetrici M, Truesdell A, Chiu C, Chiu J, et al. Chronic minocycline treatment improves hippocampal neuronal structure, NMDA receptor function, and memory processing in *Fmr1* knockout mice. Neurobiol Dis. 2018;113:11-22.
18. Pieretti M, Zhang FP, Fu YH, Warren ST, Oostra BA, Caskey CT, et al. Absence of expression of the FMR-1 gene in fragile X syndrome. Cell. 1991;66:817-822.
19. Pietropaolo S, Guilleminot A, Martin B, D'Amato FR, Crusio WE. Genetic-background modulation of core and variable autistic-like symptoms in *Fmr1* knock-out mice. PLoS One. 2011;6:e17073.
20. Lin YT, Hsieh TY, Tsai TC, Chen CC, Huang CC, Hsu KS. Conditional deletion of hippocampal CA2/CA3a oxytocin receptors impairs the persistence of long-term social recognition memory in mice. J Neurosci. 2018;38:1218-1231.
21. Bourin M, Hascoët M. The mouse light/dark box test. Eur J Pharmacol. 2003;463:55-65.
22. Deacon RM. Digging and marble burying in mice: simple methods for in vivo identification of biological impacts. Nat Protoc. 2006;1:122-124.
23. Tang S, Terzic B, Wang IJ, Sarmiento N, Sizov K, Cui Y, et al. Altered NMDAR signaling underlies autistic-like features in mouse models of CDKL5 deficiency disorder. Nat Commun. 2019;10:2655.
24. Deacon RM. Assessing nest building in mice. Nat Protoc. 2006;1:1117-1119.
25. Huang CC, Lin HJ, Hsu KS. Repeated cocaine administration promotes long-term potentiation induction in rat medial prefrontal cortex. Cereb Cortex. 2007;17:1877-1888.
26. Dansie LE, Phommahaxay K, Okusanya AG, Uwadia J, Huang M, Rotschafer SE, et al. Long-lasting effects of minocycline on behavior in young but not adult Fragile X mice. Neuroscience. 2013;246:186-198.
27. Lee CZ, Yao JS, Huang Y, Zhai W, Liu W, Guglielmo BJ, et al. Dose-response effect of tetracyclines on cerebral matrix metalloproteinase-9 after vascular endothelial growth factor hyperstimulation. J Cereb Blood Flow Metab. 2006;26:1157-1164.
28. Lin S, Wei X, Bales KR, Paul ABC, Ma Z, Yan G, et al. Minocycline blocks bilirubin neurotoxicity and prevents hyperbilirubinemia-induced cerebellar hypoplasia in the Gunn rat. Eur J Neurosci. 2005;22:21-27.
29. Kerns CM, Newschaffer CJ, Berkowitz SJ. Traumatic childhood events and Autism spectrum disorder. J Autism Dev Disord. 2015;35:3475-3486.
30. Anderson SR, Romanczyk RG. Early intervention for young children with Autism: continuum-based behavioral models. J Assoc Pers Sev Handicaps. 1999;24:162-173.
31. Hill E, Berthoz S, Frith U. Brief report: cognitive processing of own emotions in individuals with Autistic spectrum disorder and in their relatives. J Autism Dev Disord. 2004;34:229-235.
32. Duffney LJ, Zhong P, Wei J, Matas E, Cheng J, Qin L, et al. Autism-like deficits in *Shank3*-deficient mice are rescued by targeting actin regulators. Cell Rep. 2015;11:1400-1413.
33. Selimbeyoglu A, Kim CK, Inoue M, Lee SY, Hong ASO, Kauvar I, et al. Modulation of prefrontal cortex excitation/inhibition balance rescues social behavior in *CNTNAP2*-deficient mice. Sci Transl Med. 2017;9:eaah6733.
34. Antoine MW, Langberg T, Schnepel P, Feldman DE. Increased excitation-inhibition ratio stabilizes synapse and circuit excitability in four Autism mouse models. Neuron. 2019;101:648-661.
35. Sohal VS, Rubenstein JLR. Excitation-inhibition balance as a framework for investigating mechanisms in neuropsychiatric disorders. Mol Psychiatry. 2019;24:1248-1257.

36. Emadi-Kouchak H, Mohammadinejad P, Asadollahi-Amin A, Rasoulinejad M, Zeinoddini A, Yalda A, et al. Therapeutic effects of minocycline on mild-to-moderate depression in HIV patients: a double-blind, placebo-controlled, randomized trial. Int Clin Psychopharmacol. 2016;31:20-26.
37. Savitz JB, Teague TK, Misaki M, Macaluso M, Wurfel BE, Meyer M, et al. Treatment of bipolar depression with minocycline and/or aspirin: an adaptive, 2×2 double-blind, randomized, placebo-controlled, phase IIA clinical trial. Transl Psychiatry. 2018;8:27.
38. Zhang L, Zheng H, Wu R, Zhu F, Kosten TR, Zhang XY, et al. Minocycline adjunctive treatment to risperidone for negative symptoms in schizophrenia: Association with pro-inflammatory cytokine levels. Prog Neuropsychopharmacol Biol Psychiatry. 2018;85:69-76.
39. Ghaleiha A, Alikhani R, Kazemi MR, Mohammadi MR, Mohammadinejad P, Zeinoddini A, et al. Minocycline as adjunctive treatment to risperidone in children with autistic disorder: a randomized, double-blind placebo-controlled trial. J Child Adolesc Psychopharmacol. 2016;26:784-791.
40. Chini M, Pöpplau JA, Lindemann C, Carol-Perdiguer L, Hnida M, Oberländer V, et al. Resolving and rescuing developmental miswiring in a mouse model of cognitive impairment. Neuron. 2020;105:60-74.
41. Satterstrom FK, Kosmicki JA, Wang J, Breen MS, Rubeis SD, An JY, et al. Large-scale exome sequencing study implicates both developmental and functional changes in the neurobiology of Autism. 2020;180:568-584.
42. Drusenheimer N, Migdal N, Jäckel S, Tveriakhina L, Scheider K, Schulz K, et al. The mammalian orthologs of drosophila Lgd, CC2D1A and CC2D1B, function in the endocytic pathway, but their individual loss of function does not affect Notch signalling. PLoS Genet. 2015;11:e1005749.
43. Schmeisser MJ, Ey E, Wegener S, Bockmann J, Stempel AV, et al. Autistic-like behaviours and hyperactivity in mice lacking ProSAP1/Shank2. Nature. 2012;486:256-260.
44. Won H, Lee HR, Gee HY, Mah W, Kim JI, Lee J, et al. Autistic-like social behaviour in *Shank2*-mutant mice improved by restoring NMDA receptor function. Nature. 2012;486:261-265.
45. Wang X, McCoy PA, Rodriguiz RM, Pan Y, Je HS, Roberts AC, et al. Synaptic dysfunction and abnormal behaviors in mice lacking major isoforms of *Shank3*. Hum Mol Genet. 2011;20:3093-3108.
46. Yang M, Bozdagi O, Scattoni ML, Wöhr M, Roullet FI, Katz AM, et al. Reduced excitatory neurotransmission and mild autism-relevant phenotypes in adolescent Shank3 null mutant mice. J Neurosci. 2012;32:6525-6541.
47. Kwon CH, Luikart BW, Powell CM, Zhou J, Matheny SA, Zhang W, et al. *Pten* regulates neuronal arborization and social interaction in mice. Neuron. 2006;50:377-388.
48. Napoli E, Ross-Inta C, Wong S, Hung C, Fujisawa Y, Sakaguchi D, et al. Mitochondrial dysfunction in *Pten* haplo-insufficient mice with social deficits and repetitive behavior: interplay between *Pten* and *p53*. PLoS One. 2012;7:e42504.
49. Mineur YS, Huynh LX, Crusio WE. Social behavior deficits in the *Fmr1* mutant mouse. Behav Brain Res. 2006;168:172-175.
50. Garner JP, Weisker SM, Dufour B, Mench JA. Barbering (fur and whisker trimming) by laboratory mice as a model of human trichotillomania and obsessive-compulsive spectrum disorders. Comp Med. 2004;54:216-224.
51. Honey E, Leekam S, Turner M, McConachie H. Repetitive behavior and play in typically developing children and children with autism spectrum disorders. J Autism Dev Disord. 2007;37:1107-1115.
52. Kouser M, Speed HE, Dewey CM, Reimers JM, Widman AJ, Gupta N, et al. Loss of predominant *Shank3* isoforms results in hippocampus-dependent impairments in behavior and synaptic transmission. J Neurosci. 2013;33:18448-18468.
53. Kabitzke PA, Brunner D, He D, Fazio PA, Cox K, Sutphen J, et al. Comprehensive analysis of two *Shank3* and the *Cacna1c* mouse models of autism spectrum disorder. Genes Brain Behav. 2018;17:4-22.
54. Lugo JN, Smith GD, Arbuckle EP, White J, Holley AJ, Floruta CM, et al. Deletion of PTEN produces autism-like behavioral deficits and alterations in synaptic proteins. Front Mol Neurosci. 2014;7:27.
55. Gurney ME, Cogram P, Deacon RM, Rex C, Tranfaglia M. Multiple behavior phenotypes of the Fragile-X syndrome mouse model respond to chronic inhibition of phosphodiesterase-4D (PDE4D). Sci Rep. 2017;7:14653.
56. Rubenstein JLR, Merzenich MM. Model of autism: increased ratio of excitation/inhibition in key neural systems. Genes Brain Behav. 2003;2:255-267.
57. Nelson SB, Valakh V. Excitatory/inhibitory balance and circuit homeostasis in Autism spectrum disorders. Neuron. 2015;87:684-698.
58. Lee E, Lee J, Kim E. Excitation/inhibition imbalance in animal models of Autism spectrum disorders. Biol. Psychiatry. 2017;81:838-847.
59. Yizhar O, Fenno LE, Prigge M, Schneider F, Davidson TJ, O'Shea DJ, et al. Neocortical excitation/inhibition balance in information processing and social dysfunction. Nature. 2011;477:171-178.
60. Mukaetova-Ladinska EB, Arnold H, Jaros E, Perry R, Perry E. Depletion of MAP2 expression and laminar cytoarchitectonic changes in dorsolateral prefrontal cortex in adult autistic individuals. Neuropathol Appl Neurobiol. 2004;30:615-623.
61. Hutsler JJ, Zhang H. Increased dendritic spine densities on cortical projection neurons in autism spectrum disorders. Brain Res. 2010;1309:83-94.
62. Varghese M, Keshav N , Jacot-Descombes S, Warda T, Wicinski B, Dickstein DL, et al. Autism spectrum disorder: neuropathology and animal models. Acta Neuropathol. 2017;134:537-566.
63. Gao X, Zheng R, Ma X, Gong Z, Xia D, Zhou Q. Elevated level of PKMζ underlies the excessive anxiety in an Autism model. Front Mol Neurosci. 2019;12:291.
64. Hinwood M, Tynan RJ, Charnley JL, Beynon SB, Day TA, Walker FR. Chronic stress induced remodeling of the prefrontal cortex: structural re-organization of microglia and the inhibitory effect of minocycline. Cereb Cortex. 2013;23:1784-1797.
65. Pardo CA, Buckley A, Thurm A, Lee LC, Azhagiri A, Neville DM, et al. A pilot open-label trial of minocycline in patients with autism and regressive features. J Neurodev Disord. 2013;5:9.
66. Garwood CJ, Cooper JD, Hanger DP, Noble W. Anti-inflammatory impact of minocycline in a mouse model of tauopathy. Front Psychiatry. 2010;1:136.
67. Abraham J, Fox PD, Condello C, Bartolini A, Koh S. Minocycline attenuates microglia activation and blocks the long-term epileptogenic effects of early-life seizures. Neurobiol Dis. 2012;46:425-430.
68. Vargas DL, Nascimbene C, Krishnan C, Zimmerman AW, Pardo CA. Neuroglial activation and neuroinflammation in the brain of patients with autism. Ann Neurol. 2005;57:67-81.
69. Tetreault NA, Hakeem AY, Jiang S, Williams BA, Allman E, Wold BJ, et al. Microglia in the cerebral cortex in autism. J Autism Dev Disord. 2014;42:2569-2584.
70. Kern JK, Geier DA, Sykes LK, Geier MR. Relevance of neuroinflammation and encephalitis in Autism. Front Cell Neurosci. 2015;9:519.
71. Peng HZ, Ma LX, Lv MH, Hu T, Liu T. Minocycline enhances inhibitory transmission to substantia gelatinosa neurons of the rat spinal dorsal horn. Neuroscience. 2016;319:183-193.
72. Miyazaki S, Hiraoka Y, Hidema S, Nishimori K. Prenatal minocycline treatment alters synaptic protein expression, and rescues reduced mother call rate in oxytocin receptor-knockout mice. Biochem Biophys Res Commun. 2016;472:319-323.

73. Duffney LJ, Wei J, Cheng J, Liu W, Smith KR, Kittler JT, et al. *Shank3* deficiency induces NMDA receptor hypofunction via an actin-dependent mechanism. J Neurosci. 2013;33:15767-15778.
74. Pyronneau A, He Q, Hwang JY, Porch M, Contractor A, Zukin RS. Aberrant Rac1-cofilin signaling mediates defects in dendritic spines, synaptic function, and sensory perception in fragile X syndrome. Sci Signal. 2017;10:eaan0852.
75. Guo D, Peng Y, Wang L, Sun X, Wang X, Liang C, et al. Autism-like social deficit generated by *Dock4* deficiency is rescued by restoration of Rac1 activity and NMDA receptor function. Mol Psychiatry. 2019; https://doi.org/10.1038/s41380-019-0472-7